Iranica Journal of Energy & Environment

Journal Homepage: www.ijee.net

IJEE an official peer review journal of Babol Noshirvani University of Technology, ISSN:2079-2115

Preparation of iron catalysts for NO_x removal from the tail gas of HNO_3 plants

Marzieh Hamidzadeh[1,2], Aliakbar Tarlani[1], Mitra Ghassemzadeh [1]*

[1] *Chemistry and Chemical Engineering Research Center of Iran, Tehran, Iran*
[2] *Catalyst Research Group, Petrochemical Research and Technology Company, National Petrochemical Company, P.O. Box 14358–84711, Tehran, Iran*

P A P E R I N F O

Paper history:
Received 28 June 2015
Accepted in revised form 15 August 2015

Keywords:
Fe/NaY catalyst
Fe_2O_3
Zeolite
Promoters
Zeolite
NO removal

A B S T R A C T

In this paper new promoted Fe-NaY catalysts were prepared for ammonia selective catalytic reduction of NO. The prepared catalysts were characterized using X-ray diffraction (XRD), N_2 adsorption-desorption, Furrier transform infrared (FTIR) and UV–Vis diffuse reflectance spectra (UV–Vis DRS) techniques. The catalytic results revealed that among the investigated promoters (Li, Na, K, Cs, Mg, Ca, Sr, Ba, Sm, La and Ce), the K, Ba and Ca promoted Fe/NaY catalyst showed higher activity. The apparent activation energies for these catalysts are close together and change in a limited range (14.3 kJ/mol for Mg/Fe/NaY to 38 kJ/mol for Ca/Fe/NaY) because main metal ion (Fe) is fixed in all of these catalysts. The results revealed that decreasing in band gap energy in absorption edge and increasing in total acidity in the Ca/Fe/NaY, Ba/Fe/NaY and K/Fe/NaY improve the catalyst performance. In presence cerium and samarium metal ions band gap energy increased. The NO conversion on the Na/Fe/NaY, Ca/Fe/NaY and K/Fe/NaY catalysts is more than 80%.

***doi**: 10.5829/idosi.ijee.2015.06.04.05*

INTRODUCTION

Almost half of all anthropogenic NO_x emissions come from stationary sources, mainly combustion of fuels in power stations and industrial boilers while the remainder comes from mobile sources, mainly internal combustion engines [1]. In selective catalytic reduction for NO_x control, ammonia reacts with nitric oxide and nitrogen dioxide. The general reaction is as follows [2]:

$$4NO + 4NH_3 + O_2 \rightarrow 4N_2 + 6H_2O \quad (1)$$

Commercially available catalysts are based on Cu/HZSM-5 and V_2O_5/TiO_2, because these catalysts exhibit high conversions and good stability in the partially low temperature. There has been much interest in developing stable SCR catalysts in wide range temperature without toxic material such as vanadium. Many catalysts have been reported to be active for this reaction, such as transition metal oxides (e.g. Cr_2O_3-V_2O_5 [3], CuO [4], MnO_x [5], MnO_x-Fe_2O_3 [6], Fe_2O_3 [7], etc.), pillared clays and zeolites. Among these catalysts, Fe/ZSM-5 catalyst showed higher catalytic activities for the selective catalytic reduction (SCR) of NO by ammonia as compared to other known catalysts [7]. The mechanism of the reaction on the W/TiO_2 [8], vanadia/ activated semi-coke [9, 10], Cu/Bea [11], Mn/CeO_x [12] and Fe/ZSM-5 [13] catalysts have been reported.

In recent years, many studies have done on Fe/ZSM-5 catalysts for the ammonia selective catalytic reduction of NO reaction and this catalyst is consumed in industry now [13]. Although Fe/ZSM-5 catalysts showed high activity, but synthesis the NaY zeolites are cheaper than ZSM-5. Also, the NaY synthesis is free of toxic template. Therefore, we concentrate on NaY support. In this study the effect of different promoters (Li, Na, K, Cs, Mg, Ca, Sr and Ba) was investigated on the structural and catalytic properties of the Fe/NaY catalysts in NO removal reaction. Alkali or alkali earth metal ions are necessary for zeolite synthesis and in this research; we found that calcium, potassium, barium and sodium ions are better than the other metal ions in these groups for NO removal catalysts.

* Corresponding author: M. Ghassemzadeh
E-mail: mghassemzadeh@ccerci.ac.ir; Tel: +98 21 44580706, fax: +98 21 44580753.

Please cite this article as: M. Hamidzadeh, A. Tarlani, M. Ghassemzadeh, 2015. Preparation of iron catalysts for NO_x removal from the tail gas of HNO_3 plants, Iranica Journal of Energy and Environment 6 (4): 274-281.

MATERIALS AND METHODS

Materials

The starting materials were Fe $(NO_3)_3 \cdot 9H_2O$ and alkali or alkali earth nitrates as iron and promoter precursors, respectively. NaY zeolite was also used as the support of the catalyst. All reagents were used as received without further purification or additional treatment.

Catalyst preparation

Promoted Fe/ NaY catalysts with M/ Fe = 3.61 molar ratios were prepared using the impregnation method. The Si/ Al ratio in the NaY zeolite is 2.5. 18.33 g of NaY zeolite was added to an aqueous solution of a mixture of 26 mmol of alkali metal nitrate and 7.2 mmol of iron nitrate. The reaction mixture was stirred at ambient temperature for 3h. The solid mass was filtered, dried at 100 °C for 8 h and calcined at 480°C for 3 h in air atmosphere with the heating rate of 3 °C/min.

Characterization

The specific surface area was evaluated by the BET method using N_2 adsorption at –196 °C using an automated gas adsorption analyzer (NOVA 2200, Quantachrome). The Barrett, Joyner and Halenda (BJH) method was used to determine the pore size distribution from the desorption branch of the isotherm and external areas was determined using the t-plot method. In addition, the theoretical particle sizes (assuming the crystals are cubic) were calculated using the external surface area calculated from the BET method according to the equation 2 where S_{ext} is the external surface area and D_{BET} is the theoretical particle size [14]:

$$D_{\mathrm{BET}}=\frac{4061}{S_{ext}} \quad (2)$$

The crystalline structure of the prepared catalysts was determined by X-ray powder diffraction (XRD) using X-ray diffractometer (Philips diffractometer). The crystallite size of the catalysts was determined by the Debye–Scherrer equation (Eq. 3), where τ is the crystallite size, λ is the wavelength of the X-ray radiation (Cu Kά= 0.1542 nm), *k* is the shape factor (*k* = 0.94), β is the line width at half maximum height and θ is the angular position of the peak maximum [14].

$$\tau=\frac{k\lambda}{\beta cos\theta} \quad (3)$$

The Si/Al ratio can be calculated by using equation 4. [15]].

$$\frac{Si}{Al}= (25.248 - a_0)/0.245 \quad (4)$$

UV–Vis diffuse reflectance spectra (UV–Vis DRS) were recorded in air at room temperature over a range of wavelengths from 190 to 800 nm using a Shimadzu UV/VIS spectrometer. DRIFT spectra were performed in a Bruker vertex 80 FTIR instruments.

Catalytic reaction

The ammonia selective catalytic reduction of NO reaction tests was performed on a stainless steel tubular fixed bed flow reactor using 4 g catalyst. The thermocouple was inserted in the bottom of the catalyst bed to measure the reaction temperature. A gaseous mixture of 300 ppm NO, 210 ppm NH_3, 2.8% O_2 and balance N_2 were supplied to the catalyst bed and space velocity was 10000 h^{-1}.

The activity tests were carried out at different temperatures ranging from 200 ^oC to 400 ^oC in steps of 50 ^oC. The gas composition was analyzed by a gas analyzer (Testo 340). The mass reaction rate of NO removal was calculated by the equation 5:

$$r_m^{'} = -\frac{v_0}{22.4w_c} \times \frac{\varphi_{NO}}{1+\varphi_{NO}} \quad (5)$$

Where r_m' is the reaction rate ((mmole/ (g_{cat}.h)), W_c catalyst weight (g), V_0 normal flow rate of the feed (Nml/h) and φ_{NO} is a concentration of consuming nitrogen oxide in the reactor.

The catalytic activity was based on the calculated NO_x ($NO + NO_2$) conversion using the following formula:

$$NO_x \text{ conversion} = (\text{inlet } NO_x \text{ (ppm)} - \text{outlet } NO_x \text{ (ppm)} \times 100) / \text{inlet } NO_x \text{ (ppm)} \quad (6)$$

RESULT AND DISCUSSION

The textural results from nitrogen adsorption/desorption of the prepared catalysts are reported in Table 1.

In Figure. 1, the experimental isotherms follow type I isotherm where the shape of the initial part of isotherms are rather like type I but as they reach saturation, the adsorption quickly raises to a higher value (Type II). This shows a shift of micro-pore-size distribution with formation of larger micro-pores progressively filled at higher pressure. A slope at the end of the isotherms signifies the presence of meso-porous or external surface area and textural results in Table 1 confirms it. As the results, the volume of the adsorbed phase is almost limited by the volume of the micro-porosity at which the adsorption took place. Similar patterns almost appeared for nitrogen adsorption isotherm of these catalysts.

The results indicate that the isotherms almost overlap with small hysteresis, illustrating that the zeolite samples possess open and uniform micro porous system. All samples (expect Cs/Fe/NaY sample) have micro-pores by a maximum of 4 Å and meso-pores with pore

diameter between 22 to 60 Å. The micro-pores can be assigned to the channels and cavities in the zeolite crystals (4-8 Å), whereas the meso-pores loaded in metal oxide. The addition of promoters except of cesium ion did not have a significant effect on the pore size distribution of the Fe/NaY catalyst.

TABLE 1. The results of nitrogen adsorption/desorption experimental of M/Fe/NaY catalysts

Comp.	S_{BET}	S_{ext}	V_{MP}* cm^3/g	S_{Micro}	S_{Micro}/S_{BET}	S_{ext}/S_{BET}	T_P cm^3/g	Part. Size nm
Li/Fe/NaY	18 6.0	24 .7	0.0 78	16 1.4	86.77	13.2 8	0.0 94	164
Li/Fe/NaY(A)	91. 8	15 .4	0.0 36	76. 3	83.12	16.7 8	0.0 46	264
Na/Fe/NaY	16 2.1	22 .8	0.0 70	13 9.3	85.93	14.0 7	0.0 82	178
Na/Fe/NaY(A)	81. 5	10 .3	0.0 34	71. 2	87.36	12.6 4	0.0 40	394
K/Fe/NaY	75. 0	8. 2	0.0 32	66. 8	89.07	10.9 3	0.0 37	495
K/Fe/NaY(A)	10 1.3	10 .0	0.0 44	91. 2	90.03	9.87	0.0 47	406
Cs/Fe/NaY	19	9. 9	0.0 05	9.1	47.89	52.1 1		410
Cs/Fe/NaY(A)	29. 4	12 .6	0.0 08	16. 8	57.14	42.8 6	0.0 17	322
Mg/Fe/NaY	16 6.8	34 .0	0.0 64	13 2.8	79.62	20.3 8	0.0 88	119
Ca/Fe/NaY	20 1.1	24 .7	0.0 86	17 6.5	87.77	12.2 8	0.1 02	164
Sr/Fe/NaY	22 6.1	20 .7	0.0 99	20 5.4	90.84	9.16	0.1 10	196
Ba/Fe/NaY	19 1.1	10 .1	0.0 86	18 1.0	94.71	5.29	0.0 89	402
Ba/Fe/NaY(A)	13 1.3	9. 5	0.0 59	12 1.8	92.76	7.24	0.0 63	427
La/Fe/NaY	22 9.6	24 .2	0.1 01	20 5.3	89.42	10.5 4	0.1 16	168
Ce/Fe/NaY	26 9.0	30 .2	0.1 16	23 8.8	88.77	11.2 3	0.1 38	134
Sm/Fe/NaY	24 5.5	18 .7	0.1 08	22 6.8	92.38	7.62	0.1 18	217
Fe/NaY	30 8.9	60 .6	0.1 22	24 8.4	80.41	19.6 2	0.1 65	67
NaY	37 4.3	14 .2	0.1 24	36 0.1	96.21	3.79	0.1 76	286
NaY/A	29 1.9	18 .2	0.1 30	27 3.7	93.76	6.24	0.1 34	223

Particle size $= \frac{4061}{S_{ext}}$ A: After reactor , T_P : Total pore volume,

In Li/ Fe/ NaY, NaY, Ba/Fe/NaY and Na/ Fe/ NaY, it was found that surface area and micro pore volume decreased after reaction test; therefore, sintering occurred in these catalysts. Surface area of K/ Fe/ NaY and Cs/ Fe/ NaY catalysts increased after the reaction. Increasing in surface area can be attributed to removing Al atom from the frameworks, and collapsing the structure [16]. In the K/Fe/NaY catalyst some Al metal ions were replaced by Fe metal ions and the unit cell dimension of NaY decreased. Almost all of the catalysts showed shrinkage after reaction and surface area decreased. The differences in surface area are due to the complexity of accessing the surface area; therefore, pore blocking after impregnating promoters leads to low amount of nitrogen adsorbed on the catalyst.

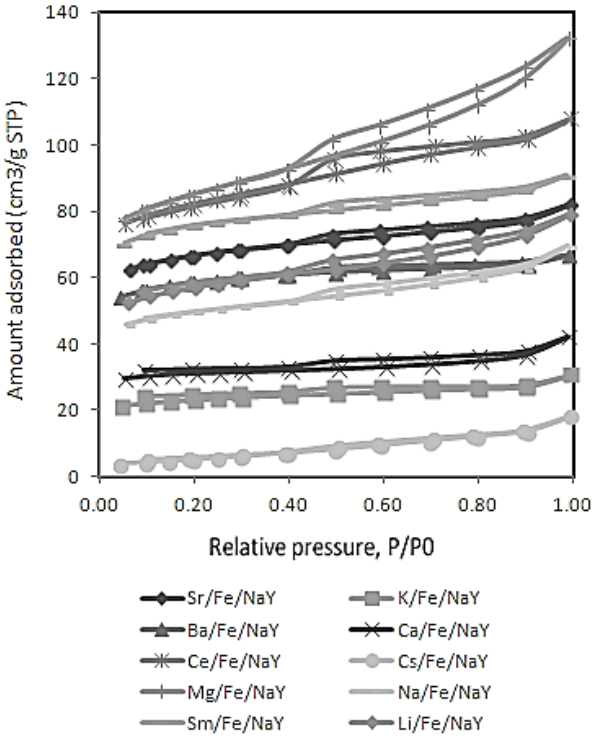

Figure 1 The experimental isotherm of nitrogen adsorption/desorption

Figure 2 shows the FTIR spectra of the fresh synthetic catalysts. The structure internal tetrahedral bending and the double ring external linkage bands were appearing between 450 to 471 cm^{-1} and 542 to 550 cm^{-1}, respectively. Similar to the literature, the later mention vibration mode in the initial NaY was shown at 560 cm^{-1} [16]. A direct correlation between the change of the wave number in the region between 400 to 500 cm^{-1} and ionic radii of cations (expect Li^+ and Mg^{2+} ions) has been found. It is confirmed by the other research [17]. Therefore, there is probably the simple electrostatic interaction between these cations and the oxygen from the framework. The shoulder at 420 to 447 cm^{-1} was attributed to opening pore of external linkage in some of these catalysts. The band intensity change could possibly be due to the interaction of hydrated cation with oxygen ring. Fe^{3+} ion is most likely to be substituted at T within TO_4 of NaY zeolite because ionic radii of dopant Fe^{3+} (0.69Å) are similar to that Al^{3+} (0.675Å). A slight shift in the shoulder at about 950 cm^{-1} towards higher frequencies probably can be attributed to replacing of Al^{3+}-ions with Fe^{3+}-ions in zeolite

structure. Al^{3+} specie was removed from the framework. The external Al^{3+} specie interacts with NO_3^- to form Al $(NO_3)_3$ species, which were converted to Al_2O_3 by calcinations. The bands about 3872 cm^{-1} and 1640 cm^{-1} were assigned to terminal silanol groups and bending vibration water in the zeolite.

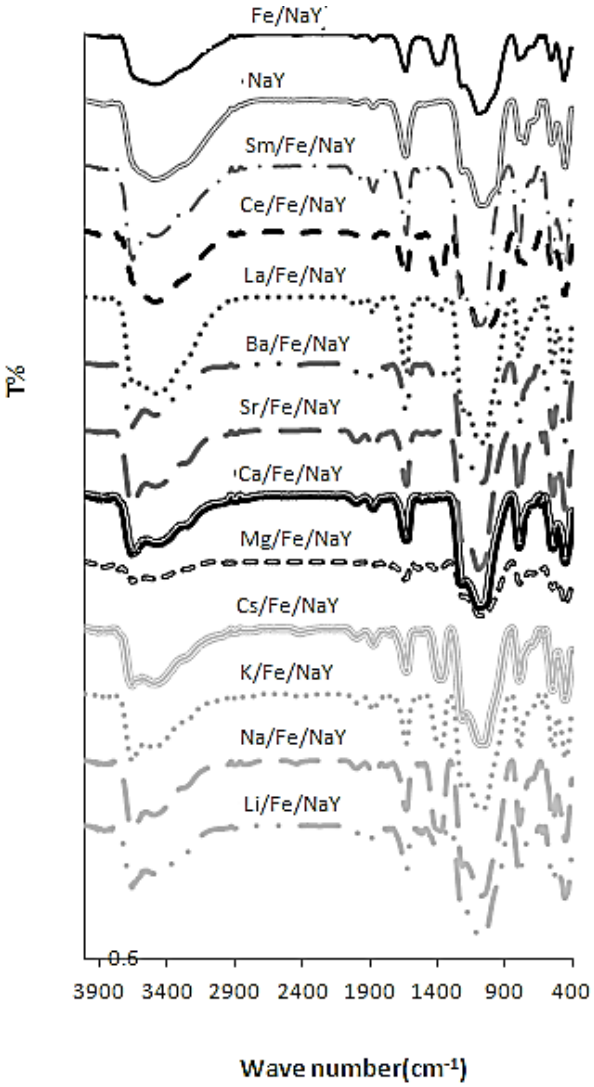

Figure 2: FTIR spectra of NaY and fresh M/Fe/NaY catalysts

The absorption bands at around 3650 cm^{-1} and 3450 cm^{-1} were associated with hydroxyl groups attached to alkali, alkali earth or rare earth ion metals and extra framework alumina (EFAL) species, respectively. The mention band is absent in the Fe/NaY catalyst and a broad band appears between 3000 to 3800 cm^{-1}. The higher catalytic activity of alkali earth metal cation exchanged Y zeolite was caused by the higher electrostatic potential of polyvalent cation and acidity of the catalysts.

By impregnation and heat treatment, the cation of metal salts not only can migrate to cages and channels in zeolite, but also react with T-OH (T = Si, Al) groups [18]. The alkali metal ions are possibly located in cages, channel or interstitial positions of the zeolite lattice and plays charge balance role. The H^+ from hydrolysis of H_2O probably attack to Al-O bond in the framework and breaks some of them when zeolite is promoted by nitrate solution [19-21].

Si from parent zeolite can convert to SiO_2 and Si/Al ratio of framework change. The FTIR spectra of Fe_2O_3 show Fe-O vibration mode in the range 400-750 cm^{-1} and have overlap by vibration modes in the zeolite support [18].

The acidic properties of M/Fe/ NaY catalysts vary in the total number of acid sites and in the strength and nature (Brønsted or Lewis) of the acid sites. Figure 3 shows NH_3-TPD profiles of fresh catalysts in the temperature range 100-900 °C. As expected, modification of Fe/ NaY zeolite by promoters influenced acid–base properties of catalyst's surface.

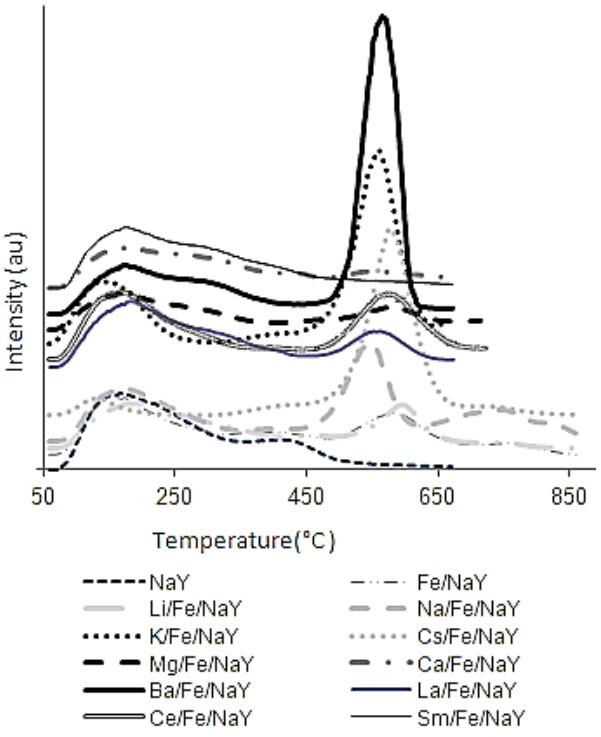

Figure 3. NH_3-TPD profiles of series M/Fe/NaY catalyst

For prompt catalysts, amount of weak, middle and strong acid surface centers determined as NH_3 consumption in the temperate region of 25 – 200 °C, 200-400 °C and 400 – 900 °C, respectively. The results of the NH_3-TPD measurements are summarized in Table 2.

Amount of weak and strong acid sites for alkali promoted catalysts decreases in the order: Cs < Li < K< Na and Cs < Li < Na < K, respectively. The alkali earth promoted samples has shown a low temperature desorption peak between 150 to 170°C with some high temperature peaks between 400 to 600°C. In Ca/Fe/NaY

TABLE 2. The results of the NH_3-TPD measurements

	Acidity strength(μmolNH_3/g catalyst)				Peak temperature(°C)	
component	W	S	S/W	Total	W	S
Li/Fe/NaY	773	1362	1.76	2135	187	611, 771
Na/Fe/NaY	2110	1206	0.6	2236	179	558,755,834
K/Fe/NaY	939	2361	2.51	3300	132	543
Cs/Fe/NaY	180	556	3.09	736	139	590,433.761
Mg/Fe/NaY	1058	537	0.51	1595	158	455,554
Ca/Fe/NaY	1289	482	0.37	1770	164,232	405,524
Ba/Fe/NaY	1466	2843	1.94	4309	156	513
La/Fe/NaY	1906	637	0.33	2543	165	525
Ce/Fe/NaY	2052	0	0	2052	158	
Sm/Fe/NaY	1557	1407	0.9	2964	148	367,537
Fe/NaY	2033	659	0.32	2692	177	443
NaY	1316	1528	1.16	2844	175	765,584,406

W: Weak acidity, S: strong acidity, T: total acidity.

sample also was appeared a middle temperature desorption peak at 232°C. The intensity of total acidity increases with increasing in ionic radii of alkali earth cations. In rare metal ions (Sm^{2+} or $Sm^{3+,}$ La^{3+} and Ce^{3+} or Ce^{4+}), total acidity increases when the charge to radius ratio of them increases. The presence of promoters changes the electrostatic field within the zeolite cavities and influence the amount of NH_3 adsorbed on surface zeolite. As the sodium cations are not fully exchanged in NaY zeolite, the presence of different cations creates a different localized electrostatic field within the zeolite pores. Hence, the difference in the adsorption characteristics would be due to the interaction between the adsorbents and different metal cations.

Although ammonia TPD profiles cannot distinguish between types of acidity, the lower temperature peak can be ascribed to ammonia desorbed from weak Lewis acid sites and the high temperature peak could be assigned to ammonia desorption from stronger Brønsted acid sites. The number of acid sites in high temperature is equal to Al in the framework, but the results are not coherent with XRD results because Si/Al ratio in XRD was calculated based on NaY zeolite phase, whilst at least two zeolite phases were distinguished in these samples. These results imply that K/ Fe/ NaY and Ba/ Fe/ NaY catalysts have more efficient acid sites for NH_3 adsorption than the other catalysts and we expected good performance in the NO removal reaction for them. However the small ionic radius and the large ionic charge in Mg^{2+} and Li^{+} can increase the effective action area between the cation and NH_3, which is positively related to the strength of their interaction. In contrast with them, Cs^{+} and Ba^{2+} ions with the largest radii in their group exhibited the higher strength of adsorption NH_3 than the upper ions in their groups in high temperature, because they located in the zeolite framework and cannot penetrate in the cages. Ammonia adsorption is the first step of NO removal mechanism; therefore, the total amount of the adsorbed NH_3 is an effective parameter in the reaction. By respect to the results in table 2, Na/Fe/NaY, K/Fe/NaY and Ca/Fe/NaY catalysts probably show good performance in comprise to the other catalysts.

In DRS-UV-Vis spectra in Figure. 4 , the absorption bands of the iron loaded NaY zeolite showed four absorption maxima at 212, 262, 356 and 495 nm. The bands below 254 nm are usually attributed to oxo-Fe (III) charge transfer (LMCT) of small Fe_xO_y clusters and exhibited strong absorption in these spectra. These transitions are responsible for a redox cycle in SCR reaction on the surface of the catalyst. The higher energy charge transfer shows that the system requires more energy for NO activation, so the conversion rate will be reduced in low temperature.

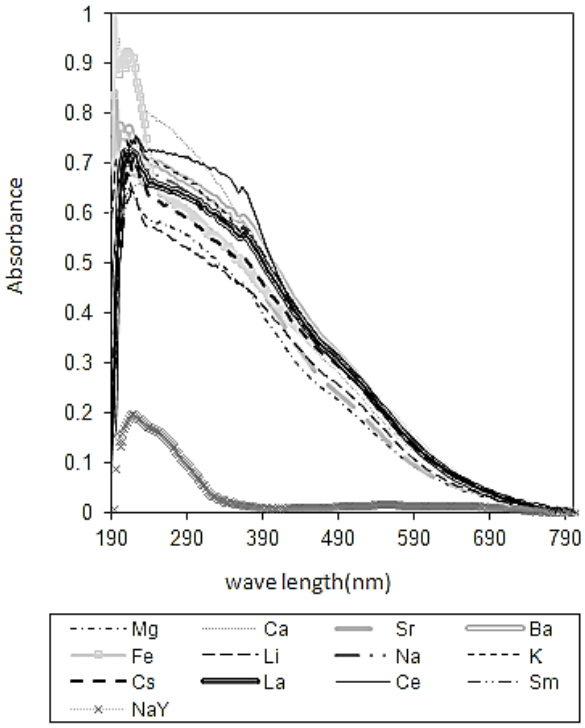

Figure 4. DRS-UV spectra of NaY and M/Fe/NaY catalysts

The absorption edge in the region from 400 to 600 nm can be assigned to the $^6A_1 \rightarrow {}^4T_2$ (4G) ligand field transition of high spin Fe^{3+} ion in tetrahedral structure. The mention bands corresponding to d-d transition and the band gap values in adsorption edge for M/ Fe/ NaY catalysts (M = alkali or alkali earth metal ions) were lower than that of bulk iron (III) oxide α-Fe_2O_3 (2.1 eV expect in Ce/ Fe/NaY) and higher than Fe/ NaY (1.8 eV) in this experimental and correspond to the literature

[22, 23]. The adsorbed NH_3 be activated by Fe^{3+} ion and the mention promoters promotes NO adsorption in the octahedral sites. By decreasing band gap energy, it is predicted that the NO removal increase. Therefore, M/ Fe/ NaY (M=Na, K, Ca and Ba) catalysts with a lower band gap in every group energy have fit properties for NO removal reaction. Two absorptions in 356 and 495 nm can be assigned to the bulk Fe_2O_3 sample and confirmed by XRD patterns [23-25]. The bands corresponding to d-d transition, which are extremely small, could not observe at around 529 to 580 nm. Also a characteristic sub-band scattering tail near 600–750 nm in some catalysts was appeared. The scattering intensity of this tail was known to increase with particle size.

The XRD results of the M/Fe/NaY samples are indicated in table 3. Two main phases were distinguished in all of them which were ZSM-5 orthorhombic structure and NaY cubic structures reported in the other literature.

TABLE 3. The calculated results of XRD data

Sample	a_0(Å)	Si/ Al	EFAL	B µmol/g	L µmol/g	B+L µmol/ g	Crystallinity %
Fe/NaY	24.53	2.9	16.8	4408.5	598.3	5006.8	
Li/Fe/NaY	24.707 13	2.2	27.9	5450.8	1523.7	6974.5	88.1
Na/Fe/NaY	24.398 75	3.5	11.0	3861.3	0	3732.9	76.1
K/Fe/NaY	24.593	2.7	20.3	4730.2	947.2	5677.4	85.9
Cs/Fe/NaY	24.865 03	1.6	42.9	6906.6	1859.1	8765.7	83.7
Mg/Fe/NaY	24.840 86	1.7	40.1	6635.4	1878.0	8513.4	84.8
Ca/Fe/NaY	24.759 23	2.0	32.1	5858.3	1727.2	7585.5	91.6
Ba/Fe/NaY	24.828 34	1.7	38.8	6503.1	1873.9	8377.0	89.2
La/Fe/NaY	24.859 86	1.6	42.3	6846.8	1866.4	8713.2	
Ce/Fe/NaY	25.009 94	1.0	65.4	9149.1	361.6	9510.7	
Sm/Fe/NaY NaY	24.819 1	1.8	37.8	6408.7	1865.7	8274.4	

EFAL=$\frac{192}{b+1}\frac{192}{c+1}$, b= global Si/Al ratio from XRF, c= framework Si/Al ratio from XRD

$$B = \frac{1}{c \times 60 + 51}$$

$$L = -0.00193 + 1.9 \times 10^{-4} \times EFAL - 2.37 \times 10^{-6} \times (EFAL)^2$$

B= Brønsted acid sites concentration , L= Lwies acid sites concentration

The alkali cations are obligatory to balance the negative charge resulting from trivalent aluminum being arranged into tetravalent configuration. These cations are not covalently bonded to the framework of zeolite and can be easily replaced with other cations without changing the zeolite structure, but in this practical research, it was observed the crystalline phase altered after impregnation iron- , alkali-, alkali earth and rare earth nitrate, therefore; the iron nitrate, low pH (3 to 4) and low stability of NaY zeolite are probably responsible for these collapse in the structure. This loss in crystallinity was confirmed by a reducing in the micro-pore and total surface area in nitrogen physisorption experiments and a shift in the symmetric strength bonds to higher wave number in FTIR spectra. As confirm our results, the higher a_0 (lattice parameter) value is parallel to the lower Si/Al ratio in NaY zeolite. Decreasing in the crystallinity and altering in XRD phase of these catalysts in comparing to zeolite parent implies the crystal structure became faulty with leaching of Al to extra framework and Si or Fe fill the skeleton vacancies of it. Reconstruction in framework confirms by observing new peak in the XRD pattern related to ZSM-5 zeolite. Trend of acid sites from XRD calculation has pretty good accommodation by NH_3-TPD and FTIR results. We could not find a relationship between B or L acidity and NO removal, but total acidity is one of the effective parameters for NO removal. According to the other results, the OH groups attached to extra framework aluminum (EFAL) species and the bridging OH groups with Brønsted acidity in FTIR were appeared about 3655 , 3500 and 3630cm^{-1}, respectively [26].

In Na/Fe/NaY, Fe/NaY and K/Fe/NaY catalysts, cell volume decreased and intensity of peaks in the XRD pattern increased, they were ascribed shirinkage in the zeolite structure.

Monomeric octahedral aqua hydroxo-complexes of iron are stable only at pH < 2 (according pourbaix curves). At higher pH values, these species tend to undergo polymerization and further precipitate *via* an olation and oxolation process. According to table 2, XRD analysis of Li/Fe/NaY and Na/Fe/NaY catalysts showed the crystalline size of 79 and 82 nm for Fe_2O_3, whereas in the K/Fe/NaY and Cs/Fe/NaY catalysts, iron contributed in mixed oxide or silicate structure. By considering SCR reaction results, Fe^{3+} is the active sites in theses catalysts.

Strong evidence exists supporting the interaction of Fe^{3+} with salicylic acid in dilute aqueous solution. According to the extracted results from XRD analysis, iron silicate phase distinguished in Cs/Fe/NaY catalyst. Therefore, it can be stated that the structure of these catalysts was not destroyed completely. When an iron ion did not replace the Al in the zeolite structure, the catalyst showed higher activity in K/Fe/NaY, Ca/Fe/NaY and Ba/Fe/NaY catalysts. Formation of extra framework Al species leads to stabilization of zeolite [27, 28].

The activation energy of the reaction was measured by changing the reaction temperature in the temperature ranges between 200-400°C. The apparent activation

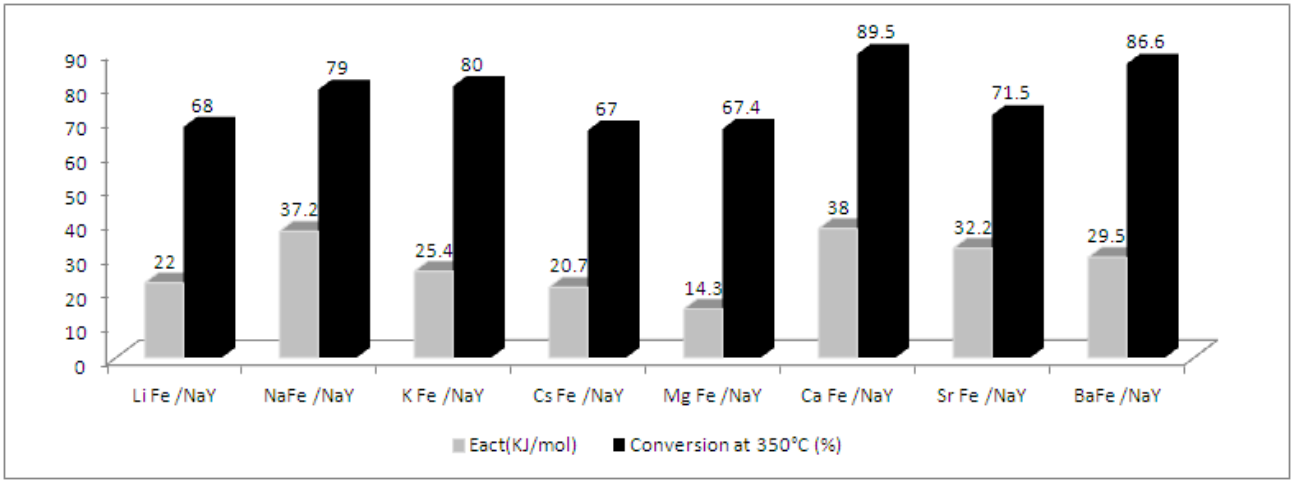

Fig.ure 5. SCR activity and apparent activation energy of fresh M/Fe/NaY catalysts: Feed gas composition is 2.6% O_2, 350 ppm NO, and 210 ppm NH_3 and space velocity is 10,000 [1/h]

energy (E_a) values were determined from the Arrhenius plots of the NO removal rate values and our results in comprise to the other author works showed good accuracy. The apparent activation energies for these catalysts are close together because main active species (Fe) are fixed in all of these catalysts [29-31].

The catalytic performances of these catalysts at 350 °C and their apparent activation energies have been shown in Figure 5

The K/ Fe/NaY, Na/Fe/NaY, Ca/Fe/NaY and Ba/Fe/NaY catalysts revealed good performance of NO removal at 350 °C. Figure 4 shows the results of the tests of catalysts in fixed bed reactor.When the temperature was too low (< 250 °C), the reaction was slow down. Maximum performance for Fe catalysts was observed in the temperature range of 330 to 380 °C. Catalyst performance was constant and acceptable for M/Fe/NaY in the temperature range of 250-400 °C.

CONCLUSION

Promoted Fe_2O_3-NaY catalysts with different alkali- , alkali earth- and earth rare metal ions were prepared by impregnation method and employed in NO selective catalytic reduction reaction. The results showed the apparent activation energies for these catalysts are close together and change in a limited range between 14- 38 kJ/mol and NO conversion of then change between 67 - 89%. Alkali earth promoter showed better performance from alkali promoter in the same period of the periodic table. The Ca/Fe/NaY, Ba/Fe/NaY and K/Fe/NaY catalysts exhibited acceptable performance in the NO

removal reaction. By decreasing in band gap energy in the absorption edge in the catalysts, by respect to promoter family, NO conversion increases. Additions of promoters have marked effect on the surface area of the catalyst; therefore, redox properties play main role in the performace of the catalysts. The results revealed that amount of acid sites and the band gap energy in this reaction controls performance of the catalyst.

ACKNOWLEDGEMENT

The authors are grateful to National Petrochemical Company, Research and Technology Company (NPC-RT) for supporting this work.

REFERENCES

1. Radojevic, M. and R.M. Harrison, Atmospheric acidity: sources, consequences and abatement. Vol. 5. 1992: Springer Science & Business Media.
2. Wijayanti, K., S. Andonova, A. Kumar, J. Li, K. Kamasamudram, N.W. Currier, A. Yezerets and L. Olsson, 2015. Impact of sulfur oxide on NH 3-SCR over Cu-SAPO-34. Applied Catalysis B: Environmental, 166: 568-579.
3. Fountzoula, C., H. Matralis, C. Papadopoulou, G. Voyiatzis and C. Kordulis, 1999. Chromia–Vanadia Catalysts Supported on TiO 2: Effect of Composition on the Physicochemical Properties and Catalytic Performance for the Selective Catalytic Reduction of NO with NH_3. Journal of Catalysis, 184(1): 5-18.
4. Baik, J.H., S.D. Yim, I.-S. Nam, Y.S. Mok, J.-H. Lee, B.K. Cho and S.H. Oh, 2004. Control of NO_x emissions from diesel engine by selective catalytic reduction (SCR) with urea. Topics in catalysis, 30(1-4): 37-41.
5. Richter, M., A. Trunschke, U. Bentrup, K.-W. Brzezinka, E. Schreier, M. Schneider, M.-M. Pohl and R. Fricke, 2002. Selective catalytic reduction of nitric oxide by ammonia over egg-shell MnO_x/NaY composite catalysts. Journal of catalysis, 206(1): 98-113.
6. Long, R.Q., R.T. Yang and R. Chang, 2002. Low temperature selective catalytic reduction (SCR) of NO with NH_3 over Fe–Mn based catalysts. Chemical Communications, (5): 452-453.

7. Qi, G. and R.T. Yang, 2005. Ultra-active Fe/ZSM-5 catalyst for selective catalytic reduction of nitric oxide with ammonia. Applied catalysis B: environmental, 60(1): 13-22.
8. Lee, S.M., S.S. Kim and S.C. Hong, 2012. Systematic mechanism study of the high temperature SCR of NO x by NH_3 over a W/TiO_2 catalyst. Chemical engineering science, 79: 177-185.
9. Nova, I., C. Ciardelli, E. Tronconi, D. Chatterjee and B. Bandl-Konrad, 2006. NH_3–NO/NO_2 chemistry over V-based catalysts and its role in the mechanism of the Fast SCR reaction. Catalysis Today, 114(1): 3-12.
10. Wang, J., Z. Yan, L. Liu, Y. Chen, Z. Zhang and X. Wang, 2014. In situ DRIFTS investigation on the SCR of NO with NH_3 over V 2 O 5 catalyst supported by activated semi-coke. Applied Surface Science, 313: 660-669.
11. Mihai, O., C.R. Widyastuti, S. Andonova, K. Kamasamudram, J. Li, S.Y. Joshi, N.W. Currier, A. Yezerets and L. Olsson, 2014. The effect of Cu-loading on different reactions involved in NH_3-SCR over Cu-BEA catalysts. Journal of Catalysis, 311: 170-181.
12. Xu, L., X.-S. Li, M. Crocker, Z.-S. Zhang, A.-M. Zhu and C. Shi, 2013. A study of the mechanism of low-temperature SCR of NO with NH_3 on MnO_x/CeO_2. Journal of Molecular Catalysis A: Chemical, 378: 82-90.
13. Ruggeri, M.P., A. Grossale, I. Nova, E. Tronconi, H. Jirglova and Z. Sobalik, 2012. FTIR in situ mechanistic study of the NH_3 NO/NO_2 "Fast SCR" reaction over a commercial Fe-ZSM-5 catalyst. Catalysis Today, 184(1): 107-114.
14. de Carvalho, M.B., A. Carvalho, F.R. Ribeiro, A. Florentino, N. Gnep and M. Guisnet, 1994. Dealumination of zeolites: Part V. Influence of the hydrothermal treatment of offretite on its pore structure and acid properties. Zeolites, 14(3): 217-224.
15. Li, P., T. Ding, L. Liu and G. Xiong, 2013. Investigation on phase transformation mechanism of zeolite NaY under alkaline hydrothermal conditions. Materials Characterization, 86: 221-231.
16. Ríos R, C.A., J.A. Oviedo V, J.A. Henao M and M.A. Macías L, 2012. A NaY zeolite synthesized from Colombian industrial coal by-products: Potential catalytic applications. Catalysis Today, 190(1): 61-67.
17. Chao, K.-j., D.-s. Shy, S.-p. Sheu and C.-f. Lin, 1994. Study of Si and Al ordering in the framework of siliceous cubic and hexagonal faujasite zeolites. Microporous Materials, 2(2): 91-104.
18. Jaafar, N.F., A.A. Jalil, S. Triwahyono, M.N.M. Muhid, N. Sapawe, M.A.H. Satar and H. Asaari, 2012. Photodecolorization of methyl orange over α-Fe_2O_3-supported HY catalysts: The effects of catalyst preparation and dealumination. Chemical Engineering Journal, 191: 112-122.
19. Fitzgerald, J.J., A.I. Hamza, C.E. Bronnimann and S.F. Dec, 1989. Solid-state 27 Al and 29 Si NMR studies of the reactivity of the aluminum-containing clay mineral kaolinite. Solid State Ionics, 32: 378-388.
20. Fitzgerald, J.J., A.I. Hamza, C.E. Bronnimann and S.F. Dec, 1997. Studies of the Solid/Solution "Interfacial" Dealumination of Kaolinite in HCl (aq) Using Solid-State 1H CRAMPS and SP/MAS 29Si NMR Spectroscopy. Journal of the American Chemical Society, 119(30): 7105-7113.
21. Zaiku, X., C. Qingling, Z. Chengfang, B. Jiaqing and C. Yuhua, 2000. Influence of citric acid treatment on the surface acid properties of zeolite beta. The Journal of Physical Chemistry B, 104(13): 2853-2859.
22. Davies, J.A., D.L. Boucher and J.G. Edwards, 1995. The question of artificial photosynthesis of ammonia on heterogeneous catalysts. Advances in Photochemistry: 235-235.
23. Mohammadikish, M., 2014. Hydrothermal synthesis, characterization and optical properties of ellipsoid shape α-Fe_2O_3 nanocrystals. Ceramics International, 40(1): 1351-1358.
24. Nedyalkova, R., S. Shwan, M. Skoglundh and L. Olsson, 2013. Improved low-temperature SCR activity for Fe-BEA catalysts by H 2-pretreatment. Applied Catalysis B: Environmental, 138: 373-380.
25. Townsend, T.K., E.M. Sabio, N.D. Browning and F.E. Osterloh, 2011. Photocatalytic water oxidation with suspended alpha-Fe_2O_3 particles-effects of nanoscaling. Energy & Environmental Science, 4(10): 4270-4275.
26. Pu, X., N.-w. Liu and L. Shi, 2015. Acid properties and catalysis of USY zeolite with different extra-framework aluminum concentration. Microporous and Mesoporous Materials, 201: 17-23.
27. Karge, H., 1998. Characterization by infrared spectroscopy. Microporous and mesoporous materials, 22(4): 547-549.
28. Pérez-Ramírez, J., M.S. Kumar and A. Brückner, 2004. Reduction of N_2O with CO over FeMFI zeolites: influence of the preparation method on the iron species and catalytic behavior. Journal of Catalysis, 223(1): 13-27.
29. Berlier, G., G. Spoto, S. Bordiga, G. Ricchiardi, P. Fisicaro, A. Zecchina, I. Rossetti, E. Selli, L. Forni and E. Giamello, 2002. Evolution of extraframework iron species in Fe silicalite: 1. Effect of Fe content, activation temperature, and interaction with redox agents. Journal of Catalysis, 208(1): 64-82.
30. Tian, W., H. Yang, X. Fan and X. Zhang, 2011. Catalytic reduction of NOx with NH_3 over different-shaped MnO2 at low temperature. J Hazard Mater, 188(1-3): 105-9.
31. Yang, J., H. Ma, Y. Yamamoto, J. Yu, G. Xu, Z. Zhang and Y. Suzuki, 2013. SCR catalyst coated on low-cost monolith support for flue gas denitration of industrial furnaces. Chemical Engineering Journal, 230: 513-521.

Persian Abstract

DOI: 10.5829/idosi.ijee.2015.06.04.05

چکیده

در این مطالعه، کاتالیست های جدید بهبود یافته Fe-NaY برای واکنش انتخابی کاهش کاتالیستی آمونیا برای NO آماده سازی شد. کاتالیست های آماده به روشهای XRD، جذب-دفع N_2، FTIR و DRS-UV-Vis ارزیابی شدند. از بین کاتایست های بدست آمده (Li، Na، K، Cs، Mg، Ca، Sr، Ba، Sm، La و Ce)، نتایج بررسی ها نشان می دهد که کاتالیست Fe/NaY بهبود یافته با K، Ba و Ca فعالیت بیشتری را نشان داده است. انرژی فعال سازی ظاهری برای این کاتالیست ها به هم دیگر نزدیک بوده و به علت جاگیری یون فلز اصلی (Fe) در این کاتالیست ها از تغییرات محدودی (۱۴٫۳ kJ/mol برای Mg/Fe/NaY تا ۳۸ kJ/mol برای Ca/Fe/NaY) برخوردار است. نتایج نشان می دهد که کاهش در انرژی باند گپ در جذب edge و افزایش در اسیدیته کلی Ca/Fe/NaY، Ba/Fe/NaY و K/Fe/NaY باعث بهبود عملکرد کاتالیست می شود. در یون فلزی سریوم و ساماریوم انرژی باند گپ افزایش یافته است. تبدیل NO بر روی کاتالیست های Ca/Fe/NaY، Ba/Fe/NaY و K/Fe/NaY نیز بیشتر از ۸۰ درصد بوده است.